BIOCHEMISTRY

When less is more: Counterintuitive stoichiometries and cellular abundances are essential for ABC transporters' function

Hiba Qasem Abdullah[1]†, Nurit Livnat Levanon[1]†, Michal Perach[1], Moti Grupper[2], Tamar Ziv[3], Oded Lewinson[1]*

Prokaryotes acquire essential nutrients primarily through adenosine triphosphate–binding cassette (ABC) importers, consisting of an adenosine triphosphatase, a permease, and a substrate-binding protein. These importers are highly underrepresented in proteomic databases, limiting our knowledge about their cellular copy numbers, component stoichiometry, and the mechanistic implications of these parameters. We developed a tailored proteomic approach to compile the most comprehensive dataset to date of the *Escherichia coli* "ABC importome." Functional assays and analyses of deletion strains revealed mechanistic features linking molecular mechanisms to cellular abundances, colocalization, and component stoichiometries. We observed four to five orders of magnitude variation in import system abundances, with copy numbers tuned to nutrient hierarchies essential for growth. Abundances of substrate-binding proteins are unrelated to their substrate binding affinities but are tightly yet inversely correlated with their interaction affinity with permeases. Counterintuitive component stoichiometries are crucial for function, offering insights into the design principles of multicomponent protein systems, potentially extending beyond ABC importers.

INTRODUCTION

Adenosine triphosphate (ATP)–binding cassette (ABC) transporters comprise one of the largest and oldest protein families of any proteome, with ~120 members in higher plants, 49 in human, and ~80 in prokaryotes. They harness the energy of ATP hydrolysis to move molecules across cell membranes (*1*). In humans, ABC transporters protect cells from toxic materials and deliver biomolecules to designated compartments. They are directly linked to human diseases and to tumor chemotherapy resistance (*2*, *3*). In prokaryotes, the high-affinity acquisition of nutrients is mediated by ABC transporters that function as importers (hereafter ABC importers). Each ABC importer is highly specific to a single nutrient or a group of highly similar nutrients. Under conditions of nutrient limitation, such as those encountered during host infection, its role is underscored. It is, therefore, not unexpected that a large number of bacterial ABC importers have been identified as key virulence determinants (*4*, *5*).

The functional unit of an ABC transporter minimally consists of four domains: two transmembrane domains (TMDs) that form the translocation pathway and two cytoplasmic nucleotide-binding domains (NBDs) that provide energy via ATP hydrolysis. ABC importers additionally require a substrate-binding protein (SBP) that binds the substrate and delivers it to its cognate transporter (*6*).

Knowledge of absolute protein levels (i.e., copy number per cell and protein cellular concentrations) is essential for kinetic modeling of biological processes for comparing concentrations of different proteins within or across samples or species and for quantifying protein-level adaptations to changes in internal or external conditions (*7*–*11*). As ABC importers provide the main route for prokaryotic nutrient import, any quantitative study of cellular metabolite influx or metabolism/anabolism balance must consider their copy number. For multicomponent systems such as ABC importers, other parameters that need to be considered are component stoichiometry and component localization/colocalization (*12*–*14*).

Bacterial ABC importers are heavily underrepresented in current proteomic datasets (*11*, *15*–*18*). In addition, in contrast to human ABC transporters (*19*, *20*) and other protein families (*21*–*25*), prokaryotic ABC importers have not been specifically targeted by proteomic studies. Therefore, we still lack a rigorous understanding of their copy number, stoichiometries, and the mechanistic implications of these parameters.

Here, we developed a tailored protocol for the label-free tandem mass spectrometry (LC-MS/MS) quantification of ABC importers and compiled a comprehensive dataset detailing their cellular copy numbers and component stoichiometries. On the basis of these proteomic data, we performed functional assays and identified unexpected mechanistic features of ABC importers, linking molecular mechanisms and physiological roles to cellular copy numbers and component stoichiometries.

RESULTS AND DISCUSSION

Compilation of the ABC importome dataset

A search of the EcoCyc database (*26*) identified 47 ABC import systems in the genome of *Escherichia coli* K12 strain BW25113. These systems, hereafter referred to as the ABC importome (table S1), are encoded by 175 genes, encoding 47 SBPs, 54 NBDs, and 74 TMDs. This composition reflects that all SBPs function as monomers. Unlike the SBPs, which function as monomers, the NBDs and TMDs function as dimers. Among the NBDs, 7 systems are heterodimeric, while 40 systems are homodimeric. The TMDs exhibit a greater tendency for heterodimerization, with 27 systems being heterodimeric and 20 being homodimeric.

[1]Department of Molecular Microbiology, Bruce and Ruth Rappaport Faculty of Medicine, Technion-Israel Institute of Technology, Haifa, Israel. [2]Infectious Disease Unit, Rambam Health Care Campus, Haifa, Israel. [3]Smoler Proteomics Center, Technion-Israel Institute of Technology, Haifa, Israel.
*Corresponding author. Email: lewinson@technion.ac.il
†These authors contributed equally to this work.

The 175 proteins that comprise the ABC importome remain underrepresented in the 18 available *E. coli* proteomic datasets (https://pax-db.org/). Moreover, reported abundances of many components can vary by up to 500-fold across different datasets. These variations may, in part, arise from the use of different growth media, as reported by Heinemann and colleagues (*11*). However, even when identical media are used, substantial discrepancies between studies persist (*16*, *27*, *28*) likely because of technical differences, including sample preparation protocols, proteolytic cleavage efficiency, detergent content, and detection sensitivity.

These inconsistencies complicate the integration of such disparate data. Therefore, our goal was to compile a unified dataset that offers a comprehensive overview of the relative abundances of the components of the ABC importome.

We used the *E. coli* K12 strain BW25113, the progenitor strain of the Keio clone collection (*29*), and a strain used in multiple proteomic investigations (*11*, *30*–*32*). Cultures were cultivated in M9-glucose medium to midexponential phase, harvested by centrifugation, and stored at −80°C until use.

Initially, LC-MS/MS analysis samples were prepared following a protocol based on SDS/urea extraction and denaturation, followed by tryptic digestion. Briefly, the extracts were dissolved in a buffer containing 10 mM dithiothreitol (DTT) and 5% SDS, sonicated, and boiled before acetone precipitation. Subsequently, the pellets were dissolved in urea/ammonium bicarbonate, reduced with DTT, and modified with iodoacetamide. Digestion was carried out overnight in the presence of urea/ammonium bicarbonate using trypsin (see Materials and Methods for full details).

As observed by others (*11*, *33*), using this standard urea-SDS-trypsin sample preparation protocol, we failed to identify many of the TMDs (table S2). Missing TMDs of special interest included those of the import systems for maltose (MalFGK), histidine (HisPQM), vitamin B_{12} (BtuCD), zinc (ZnuBC), and molybdate (MolBC).

Because the standard urea-SDS-trypsin sample preparation protocol did not lead to satisfactory coverage, we tested alternative protocols. We modified three key sample preparation parameters: (i) protease, (ii) detergent, and (iii) membrane washing agents. Beyond trypsin, we explored digestion with chymotrypsin, pepsin, LysC, WalP, and ProAnalase, all of which have been reported as promising alternatives for the proteomic analysis of membrane proteins (*34*, *35*). In parallel and in combination, we tested detergents other than SDS, such as *n*-dodecyl-β-d-maltoside (DDM), *n*-decyl-β-maltoside (DM), and their mixtures. In our experience, SDS often causes aggregation and sedimentation of ABC transporters, a problem rarely encountered with maltoside-based detergents.

In addition, we prepared membrane fractions from the same cell pellets and, for further enrichment, tested washing the membranes with high salt, EDTA, or sodium bicarbonate—agents known to remove loosely attached proteins and enhance the proteomic coverage of membrane proteins. Table S2 lists the components of the ABC importome identified using several of these alternative protocols.

The most substantial improvement came from the preparation of membrane fractions, which enabled the identification of 14 proteins previously masked by the complexity of the whole-cell proteome. Other notable improvements were achieved by washing the membranes with 100 mM sodium bicarbonate or using chymotrypsin instead of trypsin, which led to the identification of seven and nine additional components, respectively.

Unfortunately, no single sample preparation protocol achieved the desired target proteomic coverage of more than 70%. As an alternative, we chose to merge datasets obtained from different protocols. To do this, we first identified datasets with high correlation, indicating their suitability for merging.

As shown, we observed excellent correlations between technical and biological replicates (fig. S1, A and B, respectively). Furthermore, a strong correlation was evident between the intensities of membrane proteins measured in whole cells and those in membrane fractions prepared from the same cells (fig. S1C), as well as between membrane protein intensities measured in membrane fractions and those measured in the same membranes washed in 100 mM sodium bicarbonate (fig. S1D). In contrast, we observed low to moderate correlations between samples digested with trypsin and those digested with chymotrypsin, LysC, pepsin, or ProAnalase (fig. S2, A to D). Similarly, we noted low correlations between samples extracted with SDS and those extracted with DDM, DM, or a mixture of DM and DDM (fig. S3, A to C). On the basis of these findings, we concluded that MS spectra obtained from biological replicates, membrane fractions, and membrane fractions washed with sodium bicarbonate can be integrated to form a unified dataset. In contrast, spectra acquired using alternative proteases or detergents could not be reliably combined.

Subsequently, we determined the fractional mass for each protein using its relative intensity–based absolute quantification (riBAQ) values (*36*, *37*) and the known total protein content in the sample. These fractional masses were then converted to copy numbers using the molecular weights of the proteins and Avogadro's number. The ABC importome components were integrated into a consolidated dataset using the slopes of the correlation curves (fig. S1, A to D), and cellular copy numbers were derived by dividing the total copy number of each protein by the number of cells, as determined through colony counting. The complete mathematical expressions for these conversions are provided in Materials and Methods.

Next, we wished to authenticate the cellular copy numbers we determined. First, we compared our estimated cellular copy numbers with those from four other proteomic studies, which used label-free LC-MS/MS quantification (*38*, *39*), labeled peptides as internal standers (*11*), or stable isotope labeling by amino acids in cell culture quantification (*40*). For this comparison, we focused on SBPs because, unlike the TMDs and NBDs, identifying SBPs did not require additional sample processing steps (e.g., preparation of membrane fractions and membrane washing with sodium carbonate), which were only applied in our study. Figure S4 shows that our cellular copy numbers correlate reasonably with these studies [coefficient of determination (R^2), 0.61 to 0.81]. However, these correlations should be interpreted cautiously, as they are skewed by outlier data points. For instance, in fig. S4A, removing the two highest value data points reduces the R^2 from 0.81 to 0.58. Nevertheless, our study demonstrates stronger correlations with each of the four additional studies than they do with one another (compare figs. S4 and S5). Collectively, these results suggest that the quality of our comprehensive dataset is on par with what has been reported to date.

To validate the reported cellular copy numbers in a more quantitative way, we used purified proteins as standards. We chose eight components of the ABC importome that we have purified in the past. Using our established protocols (*41*–*43*), we purified three SBPs (MetQ, FliY, and BtuF), three NBDs (MetN, YecS, and BtuD),

and two TMDs (MetI and YecC), representing proteins of low, medium, and high abundance. Each protein was digested separately with trypsin, and a mixture containing equal molar amounts of the digested proteins was prepared and desalted. A sample from this mixture was then analyzed by LC-MS/MS, and the ratio between the measured intensity of each purified protein and its molar amount was used to convert the intensity measured in whole-cell samples into molar quantities. These molar amounts were then compared to the molar amounts calculated using iBAQ quantification. For complete details of how this comparison was conducted, see Materials and Methods and table S3.

As shown (Fig. 1), we observed excellent agreement between the iBAQ quantification from whole-cell lysates and the quantification using purified protein standards.

Collectively, these results suggest that the data provide a reliable estimate of the cellular copy numbers for the components of the ABC importome. Our final dataset (table S4) includes 42 SBPs, 38 TMDs, and 33 NBDs, which cover approximately 65% of the ABC importome and represent the most comprehensive coverage to date. Raw MS data are available via ProteomeXchange with identifier PXD061770.

Abundances of the components of the ABC importome

Figure 2A shows the cellular copy numbers of the SBPs we identified, and the first notable feature that we noticed was the large variation in their abundances, spanning over more than four orders of magnitude (from nanomolar to low millimolar concentrations). The most abundant SBPs, with approximately 20,000 copies per cell

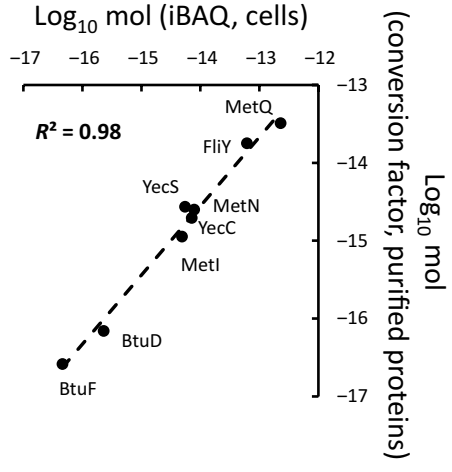

Fig. 1. High correlation between iBAQ quantification of whole-cell lysates and intensity-based quantification of purified proteins. A total of 3.45 pmol of each of the indicated proteins was trypsinized and analyzed by LC-MS/MS, as detailed in Materials and Methods. The intensity obtained for each of the purified proteins was then used to derive its "conversion factor," which is the ratio between the (known) mole amount of a given protein and its measured intensity. This conversion factor was then used to multiply the intensity values obtained for each protein in the whole-cell samples, generating a predicted mole amount that is the product of the intensity score determined in whole cells and the conversion factor determined for the purified proteins. Shown is the correlation between the amount of moles determined using the iBAQ approach in whole cells and the amount of moles calculated using the intensities measured in whole cells multiplied by the conversion factor determined using the purified proteins (*y* coordinate). The dashed line represents the linear fit, and the coefficient of determination (R^2) is indicated.

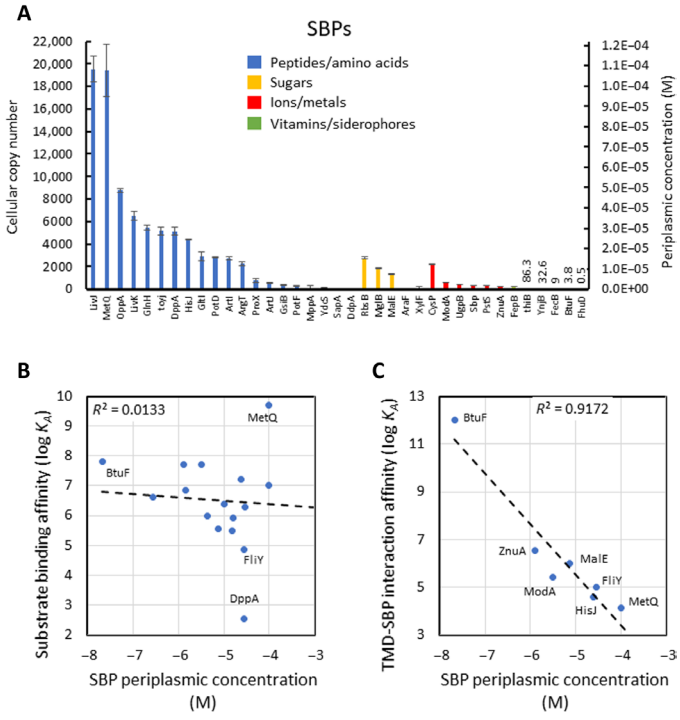

Fig. 2. Abundances and correlations of the SBPs. Shown are the cellular copy numbers of 37 SBPs, which are color coded as indicated according to their substrate group. Results are means of biological triplicates, and error bars represent SDs (**A**). Shown are the correlations between the periplasmic concentrations of the SBPs and their substrate binding affinities (**B**) or their affinity toward cognate transporters (**C**). The dashed lines represent the linear fit, and the coefficient of determination (R^2) is indicated.

(resulting in a periplasmic concentration of ~0.1 mM), were LivJ (Leu/Ile/Val SBP) and MetQ (L-Met SBP). In contrast, the least abundant SBPs, with an average of one to three molecules per cell (equating to a periplasmic concentration of approximately 2 to 6 nM), were BtuF and FhuD (B_{12} and ferric hydroxamate SBPs, respectively). To ensure that the estimated cellular copy numbers were not specific to the quantification of trypsin-derived peptides, we repeated the experiments and analyses using chymotrypsin. Reassuringly, as shown in fig. S6A, similar abundances were observed with both proteases.

We hypothesized that this substantial variability might be related to the substrate binding affinity, where high abundances could potentially compensate for low substrate binding affinities. However, as illustrated in Fig. 2B, we did not observe such a correlation. For instance, the highly abundant SBP MetQ exhibits a very high affinity for methionine (~0.2 nM) (*44*), whereas FliY, which is approximately fourfold less abundant, binds cysteine/cystine with a 50,000-fold lower affinity of ~10 μM (*43*).

An alternative driving force that may influence SBP abundance is the affinity of their interaction with their cognate transporters. SBPs that interact with low affinity may be present at higher concentrations, while those with high affinity may be present at lower concentrations. Only seven values of SBP-transporter interaction affinity have been reported to date (*41*, *45*–*49*). However, despite this paucity of information, we observed a clear correlation between the SBP-transporter interaction affinities and copy number, with high

interaction affinities strongly correlating with SBPs of low abundance and low interaction affinities strongly correlating with high SBP abundances (Fig. 2C). A similar correlation between high interaction affinity and low SBP abundance was observed when chymotrypsin was used, suggesting that this is a general phenomenon and not specific to the choice of protease (fig. S6B).

It is difficult to resolve the chicken and egg in this phenomenon: Do low SBP abundances dictate high interaction affinities with the transporter, or did high interaction affinities provide a selective pressure for reduced abundances? Whatever is the cause-effect relation, these two variables seem to be tightly linked.

In terms of abundance, the SBPs segregate into four distinct groups (Fig. 2A and fig. S6A): The most abundant SBPs are those binding peptides and amino acids. This observation aligns with the high cellular demand for amino acids (*50*) and with findings indicating that protein synthesis is the energetically most demanding cellular process (*51*). The second most abundant group consists of SBPs binding sugars, which are also required in substantial amounts. As glucose served as the carbon source for growing the cultures, the lower abundance of sugar-binding SBPs may result from carbohydrate-mediated metabolic suppression (*52*). The third most abundant group comprises SBPs for ions (e.g., phosphate, sulfate, and zinc), which are needed in smaller quantities (*53*). The least abundant SBPs are those for vitamins and siderophores, which are substances required in minute amounts. These results demonstrate that, in addition to transporter-SBP interaction affinity, substrate demand also influences the abundances of SBPs.

Similar to the SBPs, the abundances of the NBDs exhibited substantial variation, ranging from approximately 2500 copies per cell (GlnQ; involved in glutamine uptake) to around 1 copy per cell (FecE; participating in Fe^{3+}-dicitrate uptake). Their abundance hierarchy was comparable (although not identical) to that of the SBPs, i.e., peptides/amino acids > ions > sugars > vitamins/siderophores (Fig. 3A). The TMDs displayed an identical abundance hierarchy, but their estimated cellular numbers were considerably lower than those of the NBDs (Fig. 3B), which may be interpreted to suggest a stoichiometric excess of the latter. However, we could not detect any substantial amount of the NBDs in the cytosolic fractions, where their abundance was similar to that of bona fide membrane proteins, suggesting that these remnants of "cytosolic" NBDs likely stem from incomplete removal of membrane fragments from the soluble fraction. As shown later, the NBDs are membrane associated in a TMD-dependent manner. We, therefore, suggest that the apparent stoichiometric excess of the NBDs over the TMDs arises from the technical limitations of membrane protein quantification by LC-MS/MS (*54*, *55*).

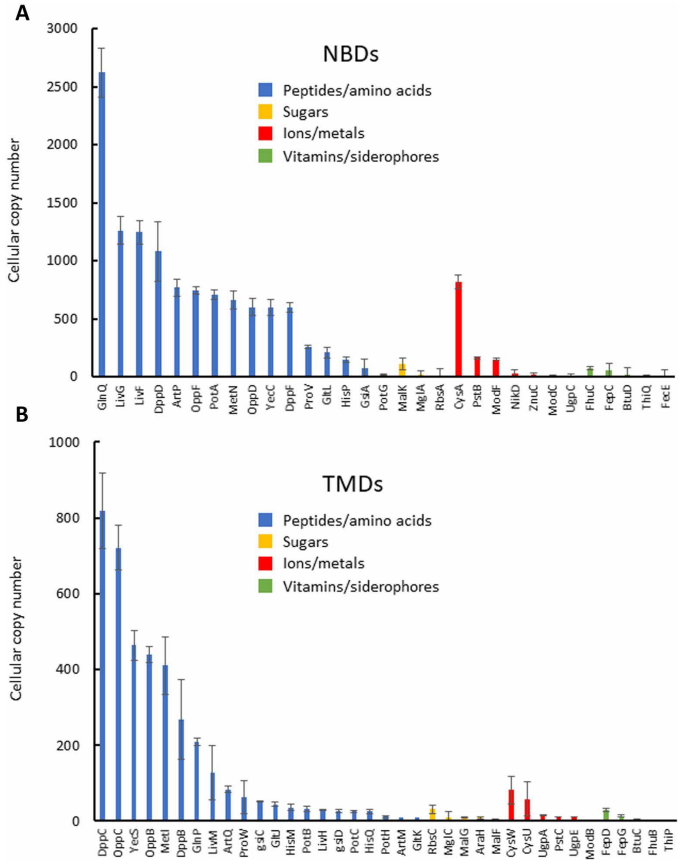

Fig. 3. Cellular abundances of the nucleotide binding and TMDs. Shown are the cellular copy numbers of 30 NBDs (**A**) and 37 TMDs (**B**), which are color coded as indicated according to their substrate group. Results are means of biological triplicates, and error bars represent SDs.

SBP-transporter stoichiometries

Another clear trend that emerges concerns the SBP-transporter stoichiometry: In all systems belonging to the type I subgroup of ABC importers (*6*, *56*), i.e., systems that import peptides, amino acids, and sugars, we observed the SBP in stoichiometric excess relative to the transporter (Fig. 4A, open bars). Similar stoichiometric ratios have been deduced from measuring protein synthesis rates (*57*). In contrast, this ratio was reversed in all type II systems (systems that import siderophores and vitamins), and the transporter was found in stoichiometric excess relative to the SBP (Fig. 4A, closed bars). We postulated that substrate availability may modulate SBP-transporter stoichiometries, where substrate presence either negatively or positively regulates component expression, thereby altering expression levels and stoichiometric ratios. To test this, we conducted experiments in the presence of various substrates. Our analysis focused on the Met, Mal, Yec, Cys, and Btu systems, which represent both type I and type II systems and span a spectrum of systems' abundances, ranging from high (Met), intermediate (Yec and Cys), and low (Mal) to very low (Btu). To ensure system saturation, substrates were added at concentrations 5- to 10-fold higher than their SBP binding affinities (*58*–*61*). For the Met system, we tested two substrates: L-methionine and D-methionine. Both are recognized by the SBP (MetQ) and inhibit the adenosine triphosphatase activity of the transporter by binding to its cytoplasmic regulatory domain (*62*). However, the proteinogenic L-isomer is imported with much higher affinity (*44*). As shown in Fig. 4B, the expression levels of the system's components and, consequently, their stoichiometry remained largely unaffected by both the inhibitory and transported substrates. Similar results were observed for the Btu (Fig. 4C) and Mal (fig. S7A) systems, where the expression levels of the system's components and their stoichiometry remained unchanged in the presence of the transported substrate. In our experiments with the Cys and Yec systems, we tested two related substrates: L-cysteine and its oxidized dimer derivative, L-cystine. Both substrates are recognized and imported by the Yec system

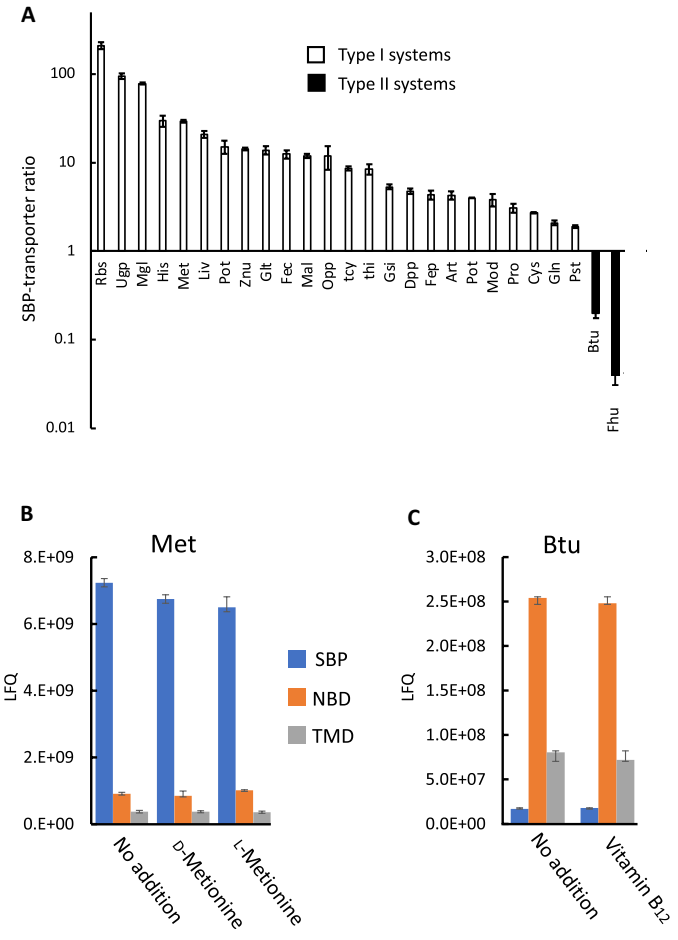

Fig. 4. Different SBP-transporter stoichiometries in type I and II systems. Shown are representative SBP-transporter stoichiometries determined for type I (open bars) and type II systems (full bars). Results are means of biological triplicates, and error bars represent SDs (**A**). Shown is the label-free quantification (LFQ) of the abundances of the components (SBP, blue; NBD, orange; TMD, gray) of the Met (**B**) and Btu (**C**) systems determined for cells grown in minimal medium in the absence ("no addition") or presence of 20 μM D-methionine, 1 nM L-methionine, or 50 nM B_{12}, as indicated. These concentrations correspond to 5- to 10-fold excess relative to the substrate binding affinities of the SBPs (*45*, *60*). Results are means of biological triplicates, and error bars represent SDs.

and are linked to the regulation of the expression of the Cys system (*43*, *61*, *63*). Our results showed that the expression levels of all three components—SBP, NBD, and TMD—in both cysteine-related systems were markedly reduced in the presence of L-cysteine and L-cystine, with L-cystine exerting stronger repression (fig. S7, B and C). Despite these changes in expression levels, the stoichiometric ratios between the components remained relatively constant, with the SBP-transporter stoichiometry in the Yec and Cys systems consistently greater than 1 (fig. S7, B and C).

These findings suggest that, although there is some variability among different systems, the SBP-transporter stoichiometry is a robust parameter inherent to these systems and is largely unaffected by the presence or absence of substrate.

As shown in Fig. 4A, in type II systems, the SBP-transporter stoichiometry is <<1, and this ratio is substrate independent (Fig. 4C). This is a very unusual observation that raises questions about the relevance of in vitro transport assays conducted with such systems, which assume that the SBP-transporter stoichiometric ratio is >>1 (*42*, *49*, *64*–*66*). At this point, we can only speculate about the forces that shaped the different SBP-transporter stoichiometries in type I and type II systems. Possibly, the higher interaction affinities between the SBP and the transporters in type II systems necessitated their reduced stoichiometry. Support for this idea is presented in the "Mechanistic implications of SBP-transporter stoichiometries" section, which highlights the functional implications of this unexpected stoichiometry.

Interdependence of expression and membrane localization

When comparing whole-cell lysates to membrane fractions prepared from the same cells, we observed a five- to sixfold enrichment in the fractional abundances of the TMDs (see the slope of the linear fit in fig. S1C). This enrichment factor is somewhat greater than the one expected based on the fraction of membrane proteins in *E. coli* (20 to 25%) (*67*) and possibly reflects the non-monotonous technical improvement in detecting membrane proteins associated with reduced sample complexity (*68*). In contrast, the SBPs were heavily underrepresented in the membrane fraction. This is not unusual given the stoichiometric mismatch between the SBP and the transporter in type I systems and considering that the periplasm is discarded during membrane preparation. However, there were three exceptions to this trend, and the SBPs MetQ, BtuF, and FhuD were enriched in the membrane fraction (Fig. 5). For MetQ, the SBP of the methionine import system, this is not unusual because MetQ is uncharacteristically tethered to the membrane via a lipid anchor (*69*, *70*). BtuF and FhuD, on the other hand, are "regular" periplasmic proteins that do not contain a membrane-anchoring domain. Nevertheless, FhuD and BtuF were not detected in the periplasm and were exclusively membrane bound. This finding challenges the prevailing dogma that periplasmic diffusion of SBPs is a fundamental aspect of the ABC transport mechanism.

The membrane association of BtuF and FhuD could be a result of a direct interaction with membrane lipids (as is the case of MetQ), a specific interaction with their cognate TMDs, or interactions with

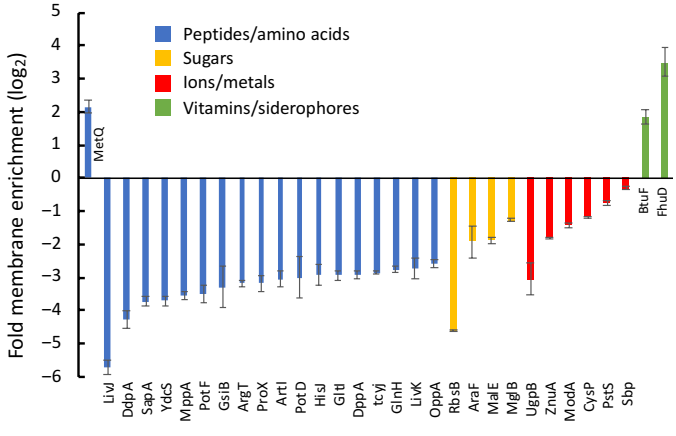

Fig. 5. SBPs of type II systems are membrane bound. Shown (in $\log_2$ scale) are the ratios between the abundances of the SBPs in whole-cell lysates versus their abundances in the membrane fraction. Results are means of biological triplicates, and error bars represent SDs.

an unknown membrane protein(s). To distinguish between these possibilities, we repeated the experiments with strains carrying chromosomal deletions of the cognate TMDs of eight different import systems. In terms of total expression levels, the SBPs were not deleteriously affected by the deletion of their cognate TMDs (Fig. 6A). Notably, the expression of the SBPs for molybdate (ModA) and zinc (ZnuA) increased 20- and 30-fold, respectively, upon deletion of the corresponding TMDs. We suspect that this represents a substrate-specific starvation response. The cellular requirement of both zinc and molybdate cannot be compensated for by alternative systems. In contrast, SBPs that were not induced by deletion of their TMDs are either of systems that can be complemented by alternative sugars/amino acids/peptides (e.g., His, Mal, Yec, and Met) or not essential under these growth conditions (Fhu and Btu).

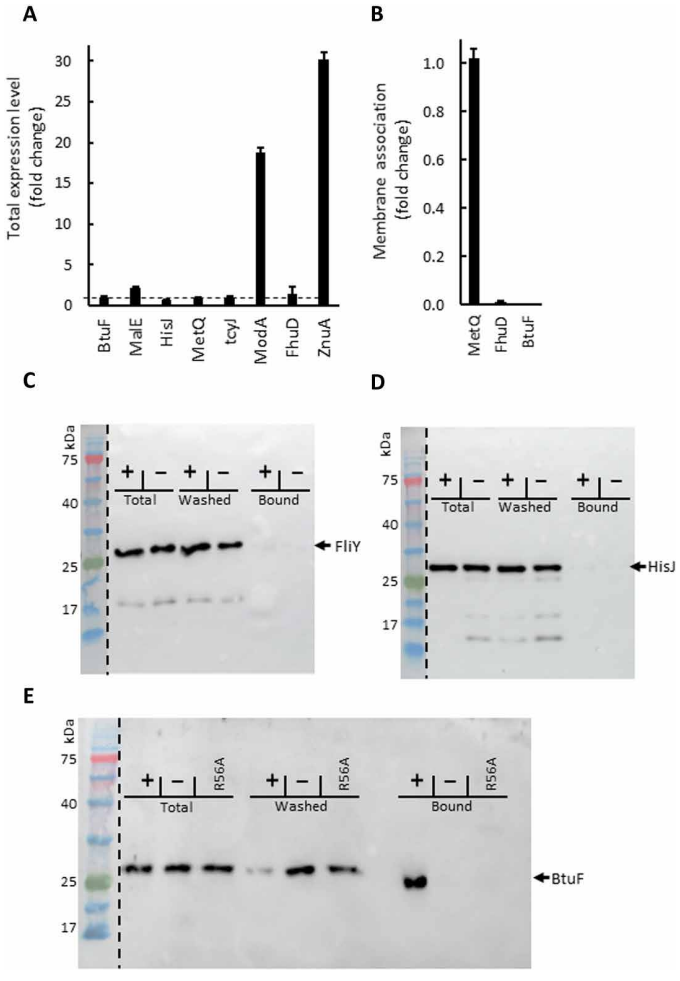

Fig. 6. Colocalization of SBPs and TMDs in type II systems. (**A** and **B**) Shown is the fold change in the abundances of the indicated SBPs following deletion of their cognate TMDs measured in total cell lysates (A) and membrane fractions (B). Shown are fold changes. Error bars represent SDs, and results represent the mean of biological triplicates. (**C** to **E**) Cells deleted of the indicated TMDs were transformed with an empty plasmid or one harboring the deleted TMD (− and +, as indicated). Cells were then permeabilized by mild osmotic shock, and purified SBPs were added at concentrations ×10 their K_D of interaction with their cognate transporters. Following a 15-min incubation, bound and unbound SBPs were separated by a wash step. Shown are immunoblots of SDS–polyacrylamide gel electrophoresis of the total, washed, and cell-bound fractions for the type I systems Yec (C) and His (D) and for the type II system Btu (E). For the Btu system, an additional negative control was provided by cells that expressed the R56A mutant of BtuC that does not interact with BtuF. The dashed lines mark the boundary between the fluorescent and visible light images merged to create the composite image.

Next, we tested whether the membrane association of MetQ, BtuF, and FhuD depended on their interactions with cognate TMDs. Deletion of the TMD MetI had no effect on the membrane association of its cognate SBP, MetQ (Fig. 6B). This result is expected, as MetQ is the only *E. coli* SBP directly anchored to the membrane via covalent lipidation (*69*).

In contrast, the stable membrane association of BtuF and FhuD, both type II system SBPs, was entirely dependent on the presence of cognate TMDs: Upon deletion of these TMDs, the cellular copy numbers of BtuF and FhuD remained unchanged (Fig. 6A), but their membrane association was completely lost (Fig. 6B), demonstrating that this localization was mediated through specific SBP-TMD interactions. This stable and specific association between SBPs and TMDs in type II systems challenges the assumption that cyclic association-dissociation of SBPs is essential for transport by ABC importers.

To complement these studies, we performed membrane association biochemical assays. In these experiments, we permeabilized the outer membrane of the cells by a mild osmotic shock treatment (see Materials and Methods). We then added purified SBPs, incubated, and washed the cells. Our rationale was that SBPs that freely diffuse in the periplasm will be removed by this wash step, while those that are firmly membrane associated will not. We tested two type I SBPs, HisJ and FliY, and observed that they were removed by the wash step (Fig. 6, C and D), which are in line with the proteomic data that show that SBPs of type I systems are not membrane associated. In contrast, and in line with the membrane enrichment observed for type II SBPs (Fig. 5), BtuF remained membrane associated despite the wash step (Fig. 6E). In addition, in line with the proteomic data was the finding that the membrane association of BtuF fully depended on the expression of its cognate TMDs (Fig. 6E). These complementary biochemical studies further suggest that SBPs and TMDs in type II systems associate very tightly, potentially remaining bound without dissociating.

Similar to the SBPs, the NBDs did not exhibit detrimental effects on total expression levels upon the deletion of their corresponding TMDs. In contrast, most NBDs demonstrated an increase in expression when their TMDs were absent (Fig. 7A). The only exception was observed with MetN, which completely failed to express in the absence of MetI. This, coupled with the distinct membrane tethering of MetQ, indicates that the methionine system is an exceptional case. Despite the heightened expression levels, the NBDs could hardly be detected in the membrane fraction (Fig. 7B). This implies that, while the NBDs do not necessitate their corresponding TMDs for expression per se, they are absolutely dependent on them for membrane association.

Our collection of deletion strains included two transporters with heterodimeric TMDs: the histidine transporter $HisP_2QM$ and the maltose transporter $MalFGK_2$. The structures of $MalFGK_2$ (*71*) show that MalF and MalG are highly asymmetric, each contributing a different subset of residues to the translocation pore and to the interaction surface with the SBP. The consensus is, therefore, that this heterodimeric organization is an inherent and essential property of such transporters. To our great surprise, MalF was still present in the membranes of the Δ*malG* strain, and as if to compensate

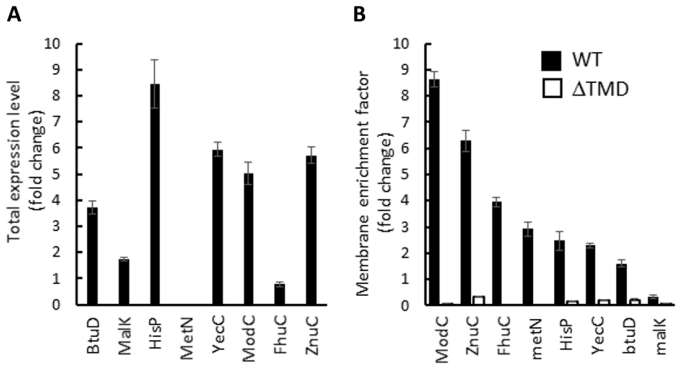

Fig. 7. TMD-dependent expression and membrane localization of the NBDs. Shown is the fold change in the total expression level (i.e., abundance determined in whole-cell extracts) of the indicated NBDs upon deletion of their cognate TMDs (**A**). Shown is the membrane enrichment factor of the indicated NBDs measured in wild-type (WT) (full bars) or ΔTMD cells (open bars) (**B**). Error bars represent SDs, and results represent the mean of biological triplicates.

for the *malG* deletion, the amount of MalF increased almost exactly twofold (fig. S8A). In contrast, we could not detect MalG in the membranes of cells deleted of *malF* (not shown). These results suggest that MalF can insert into the membrane independently of MalG and not vice versa. In line with these observations, the membrane association of MalK (the NBD of the maltose transporter) was hardly affected by the absence of MalG but was nearly completely abolished in the absence of MalF, indicating that the expression of MalF is sufficient and essential for the membrane association/localization of MalK (fig. S8B). A somewhat similar phenomenon was observed with the histidine transporter HisPQM. Both HisM and HisQ (the TMDs) were detected in the absence of their counterpart. Of the two, HisQ was less dependent on HisM than vice versa, and its expression in the membranes of Δ*hisM* cells was ~5-fold higher than that of HisM in Δ*hisQ* cells (fig. S8C). Notably, HisP (the NBD) was readily detected in membranes devoid of HisM but was completely absent from those devoid of HisQ (fig. S8C). The above observations raise the possibility that these heteromeric transporters may also form stable homomeric membrane-bound complexes (i.e., $MalF_2K_2$ and $HisQ_2P_2$), a suggestion that requires further investigation.

Mechanistic implications of SBP-transporter stoichiometries

As shown in Fig. 4, all type I systems exhibited a stoichiometric excess of the SBP in the range of 10- to 200-fold over the transporter. Notably, in the case of the type I maltose transporter, this surplus of the SBP has been established as crucial for activity. Mutations in the signal sequence of the SBP (MalE), which reduce its export to the periplasm and consequently lower its periplasmic copy number, lead to a decrease in transport rates. This reduction in transport rates results in impaired utilization of maltose as a carbon source (*72*, *73*). It appears, therefore, that in systems involved in the transport of abundantly available biomolecules, particularly those required in substantial quantities such as carbohydrates and amino acids, the stoichiometric excess of the SBP represents an essential mechanistic feature.

Unexpectedly, and perhaps counterintuitively, type II systems exhibited a reversed ratio, with the transporter found in 10- to 100-fold stoichiometric excess over the SBP (Fig. 4A), and this stoichiometry persisted both in the presence and in the absence of substrate (Fig. 4C).

To assess the implications of the "reversed stoichiometry" observed in type II systems, we adjusted the SBP ratio in the Btu system by increasing the expression of the SBP (see Materials and Methods for details). LC-MS/MS analysis confirmed that this adjustment, referred to as $BtuF_{high}$, replicates the SBP-transporter stoichiometric ratio observed in type I systems, characterized by an approximately 100-fold excess of SBP. The only modification introduced was the alteration of this stoichiometric ratio, with all other mechanistic aspects of the Btu system remaining consistent with the wild-type (WT) system.

For these experiments, we used an *E. coli* strain that can synthesize methionine exclusively through B_{12}-dependent catalysis (*42*). As a result, this strain can only grow in media supplemented with either methionine or B_{12}. When B_{12} is provided, the high-affinity uptake activity of the BtuCD-F system becomes crucial for its growth.

In media supplemented with methionine, we observed no distinction between WT cells expressing the intrinsic low levels of BtuF (referred to as $BtuF_{low}$) and those expressing $BtuF_{high}$ (Fig. 8A). Subsequently, we replicated these experiments, but instead of methionine, we supplemented the media with a surplus of B_{12}. As shown in Fig. 8B, in the presence of high concentrations of B_{12} that support 100% growth (compare Fig. 8, A and B), the elevated expression of the SBP did not confer either a growth advantage or a disadvantage. As we lowered the concentrations of B_{12}, making it limiting for growth, the $BtuF_{low}$ cells exhibited a substantial growth advantage, and this advantage became more pronounced as the concentrations decreased (Fig. 8, C to F). This stands in stark contrast to the observations for the model type I transporter MalFGK-E, where reduced SBP led to decreased transport and impaired growth (*72*, *73*).

A link between thermodynamics, conformational dynamics, copy number, and component stoichiometry

The unexpected phenomenon, where increasing amounts of one of the components of a system lead to reduced output, can be explained by considering the thermodynamics and physiological role of systems such as Btu. The physiological role of such type II systems is to import scarce nutrients, requiring the SBP to have a very high binding affinity (*56*). For such high-affinity ligand binding, evolution has favored a lock-and-key mechanism: The ligand-binding site in the SBP is mostly preformed and undergoes minimal structural rearrangement upon ligand binding (Fig. 9, left). As a result, the ligand-free and ligand-bound conformations of the SBP are similar (*74*, *75*). Consequently, the transporter cannot readily differentiate between the ligand-free and ligand-bound SBP, and under normal physiological concentrations, both bind to it with high affinity (Fig. 9, left) (*41*). This contrasts with type I systems, where a substantial conformational change in the SBP occurs upon ligand binding (*56*), allowing the transporter to distinguish between the ligand-free and ligand-bound forms (Fig. 9, right).

Although the nutrients imported by type II systems are essential for growth, they are needed in small amounts. For example, as established in previous observations (*42*), and further corroborated by our findings (Fig. 8B), as little as 5 nM B_{12} supports maximal growth.

This concentration corresponds to a periplasmic presence of approximately three to four B_{12} molecules, perfectly aligning with the cellular copy number of BtuF (four copies per cell; table S4). The cellular copy number of the transporter is approximately 20 (table S4), leading to an SBP-transporter stoichiometry of <1 (Fig. 10, top left). Under these conditions, transporter docking sites are available

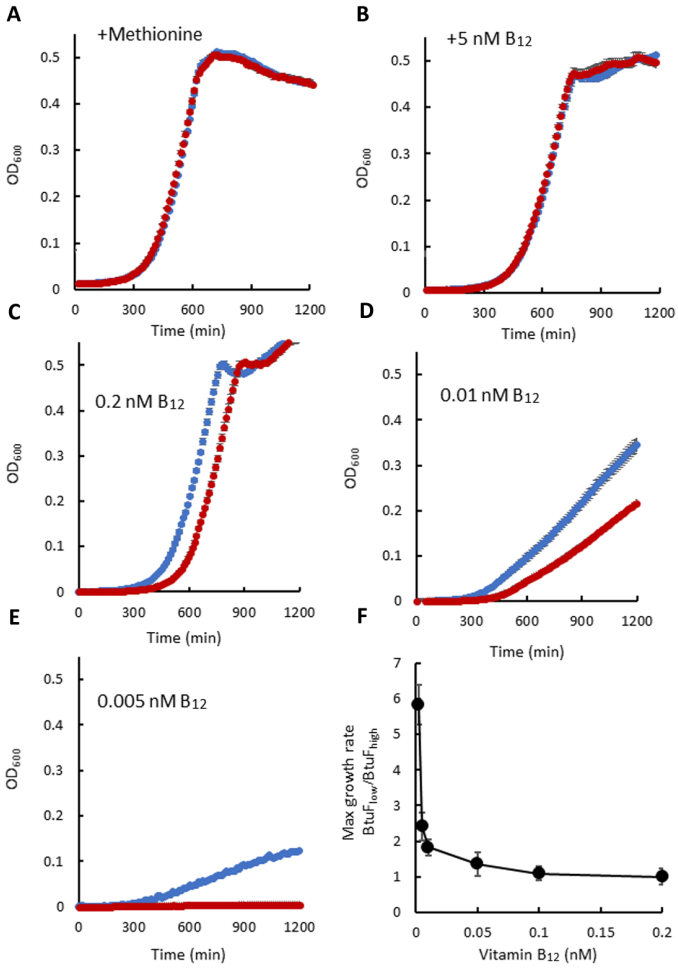

Fig. 8. Unexpected advantage of SBP-transporter stoichiometry <1. Δ*metE* cells rely on B_{12}-dependent enzymatic methionine synthesis. Cell growth is contingent on exogenous methionine or B_{12}, with BtuCD-F facilitating the import of the latter (*42*, *59*). Δ*metE* cells were cultured in the presence of 20 μg/mL methionine (**A**) or the indicated concentrations of vitamin B_{12} (**B** to **E**). Shown is the growth of cells with natural ($BtuF_{low}$; blue curves) and elevated ($BtuF_{high}$; red curves) BtuF levels. In (**F**), the ratio of the maximal growth rate between $BtuF_{low}$ and $BtuF_{high}$ cells is presented as a function of B_{12} concentrations. Notably, under B_{12} limitation, $BtuF_{low}$ cells exhibit approximately sixfold faster growth than $BtuF_{high}$ cells; under B_{12} abundance, growth is identical. Results are averages of biological triplicates, with error bars indicating SDs. OD, optical density.

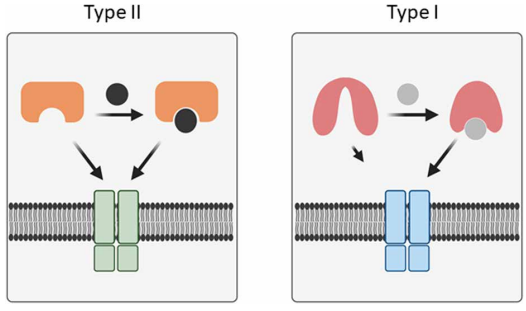

Fig. 9. Different modes of ligand binding by type I and type II SBPs. Type II SBPs (left) undergo minimal structural rearrangement upon ligand binding. As a result, the transporter cannot readily distinguish between the ligand-free and ligand-bound forms of the SBP, and both bind to it with high affinity. In contrast, type I SBPs (right) undergo substantial structural rearrangement following ligand binding, and the transporter preferentially interacts with the ligand-bound form. This image was created with BioRender.com.

for all B_{12}-bound BtuF molecules, and import is normal. In the manipulated system ($BtuF_{high}$), the SBP-transporter stoichiometry is >1 (Fig. 10, top right). Under these conditions, the expression of excess BtuF relative to B_{12} leads to the generation of a population of B_{12}-free BtuF molecules. Previous studies have demonstrated that B_{12}-free BtuF exhibits very high affinity toward its cognate transporter (*41*). Consequently, these ligand-free BtuF molecules will compete with the fewer ligand-bound ones for docking to the available transporters (Fig. 10, top right). Given their extremely slow dissociation rate (~10^{-7} s^{-1}) (*41*), this will effectively clog the system and reduce uptake rates, as demonstrated in Fig. 8 (C to F). A similar problem does not arise in type I systems (Fig. 10, bottom). Their substrates are sufficiently abundant to saturate the SBPs, diminishing the competition between substrate-free and substrate-loaded SBPs (Fig. 10, bottom right). In addition, type I transporters preferentially associate with substrate-loaded SBPs, and their SBPs rapidly dissociate from the transporters, avoiding the problem of clogging the transporters with substrate-free SBPs (*41*, *45*–*47*). As shown previously (*72*, *73*), low expression of type I SBPs leads to reduced uptake (Fig. 10, bottom left), in direct contrast to type II systems (Fig. 10, top left).

It therefore seems that two different SBP-transporter stoichiometries evolved, with ratios >1 and <1 tailored for acquiring biomolecules of high and low abundance, respectively.

How is expression regulated?

Many import systems are expressed at substantial levels even in the absence of their specific substrates in the growth medium (e.g., Met, Liv, and His; Figs. 2 and 3). This observation suggests that many systems are constitutively expressed, remaining in a state of readiness for the appearance of their substrates. Such a strategy eliminates the need for the time-consuming processes of transcription, translation, membrane insertion, and complex assembly, which could result in missed import opportunities.

In cases where excessive import of the substrate is toxic (e.g., zinc and nickel), expression is tightly controlled by substrate-responsive transcriptional elements (*76*, *77*). However, the findings presented in Fig. 4 (B and C) and fig. S7A suggest that direct substrate–mediated feedback regulation does not apply to certain systems, raising questions about the mechanisms governing their expression.

An alternative explanation could link expression to broader physiological states. For carbohydrate importers, expression might be tied to the cell's energetic balance. Similarly, for peptide and amino acid importers, the general availability of these nutrients could influence their expression levels. A comprehensive approach integrating multiple omics techniques—such as transcriptomics, proteomics, and metabolomics—could provide a holistic understanding of the factors driving the expression of these import systems.

In summary, we integrated proteomic analysis with functional assays to explore correlations between thermodynamic/kinetic properties, substrate specificity, copy number, and component stoichiometry in ABC import systems. Our findings reveal abundances that vary over four to five orders of magnitude and correlate with the quantities of nutrients requiring acquisition. In addition, we observed

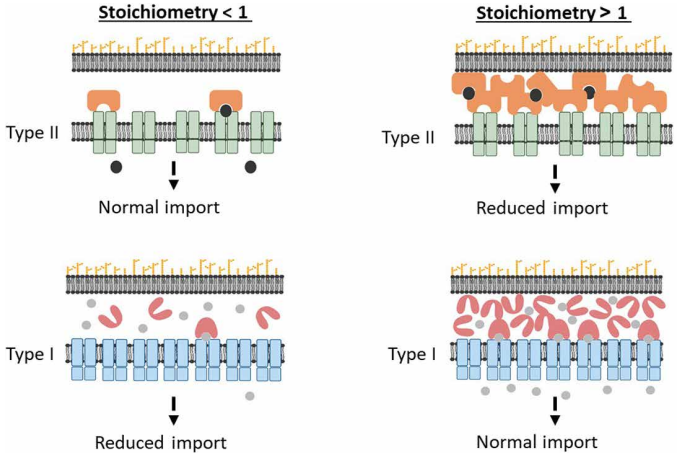

Fig. 10. SBP-transporter stoichiometries <1 are adapted to transporting scarce nutrients. Type II systems, which import scarce compounds such as vitamins, function optimally when the SBP is present in stoichiometric paucity relative to the transporter (top left). Because of the limited environmental availability of ligands, an excess of SBP leads to a large population of ligand-free SBPs that compete with ligand-bound ones for transporter interaction, resulting in reduced uptake (top right). In contrast, type I systems, which import abundant compounds such as amino acids, perform best when the SBP is in stoichiometric excess relative to the transporter (bottom right). In these systems, excess SBP does not pose an issue because the transporter-SBP complex is inherently unstable, and the transporter preferentially interacts with substrate-loaded SBPs. However, in type I systems, a paucity of SBP results in fewer ligand-binding events, fewer successful transporter-SBP interactions, and reduced import (bottom left). This image was created with BioRender.com.

that receptors (SBPs) of systems importing rare compounds do not freely diffuse in the periplasm but are firmly docked to their cognate membrane–embedded transporter. The tight association between type II SBPs and their cognate TMDs raises the possibility that transport in these systems may occur without the SBP ever dissociating. While this idea is intriguing, to the best of our knowledge, experimental evidence supporting its existence is still lacking. Notably, such systems use a reversed stoichiometry, where the receptor is found in paucity relative to the transporter. Together, the results showcase correlations between physiological roles, molecular-level attributes, and cellular-context parameters, suggesting their coevolution to optimize the output of multicomponent systems.

MATERIALS AND METHODS

MS sample preparation and data analysis

Cultures of the *E. coli* K12 strain BW25113, the progenitor strain of the Keio clone collection (*29*), were grown to midexponential phase in M9 liquid medium containing 42.2 mM Na_2HPO_4, 22.0 mM KH_2PO_4, 8.6 mM NaCl, 18.7 mM NH_4Cl, 1% thiamine, 1 mM $MgSO_4$, 10 μM $CaCl_2$, 0.025% arginine, 0.025% lysine, and 0.5% glucose. Cells were harvested by centrifugation, washed in phosphate-buffered saline, and stored at −80°C. Where indicated, membranal, cytosolic, and periplasmic fractions were prepared from these cell pellets. For the preparation of the membrane fraction, cells were resuspended in 50 mM tris-HCl (pH 7.5) and 0.5 M NaCl and ruptured by tip sonication (3 s by 20 s, 600 W). Debris and unbroken cells were removed by centrifugation (10 min, 10,000*g*), and the membranes were pelleted by ultracentrifugation at 120,000*g* for 45 min. The membranes were washed and resuspended in 50 mM tris-HCl (pH 7.5) and 0.5 M NaCl and stored at −80°C. Where indicated, membranes were subjected to an additional wash step with 100 mM sodium bicarbonate, 2 M sodium chloride, or 25 mM EDTA.

Next, the samples were dissolved in 10 mM DTT, 100 mM tris-HCl, and 5% SDS or 1% DDM, 1% DM, or a mixture of 1% DDM + 1% DM, as indicated. Samples were sonicated and boiled at 95°C for 5 min and precipitated in 80% acetone. The protein pellets were dissolved in 9 M urea and 400 mM ammonium bicarbonate, then reduced with 3 mM DTT (60°C for 30 min), modified with 10 mM iodoacetamide in 100 mM ammonium bicarbonate (room temperature and 30 min in the dark), and digested overnight in 2 M urea and 25 mM ammonium bicarbonate at 37°C using a 1:50 (mol/mol) of modified trypsin (Promega), 1:10 (mol/mol) chymotrypsin (Roche), 1:50 (mol/mol) ProAnalase (Promega), 1:50 (mol/mol) WalP (Cell Signaling Technology), 1:3 (mol/mol) pepsin (Promega), or 1:50 (mol/mol) Lys-C (Fujifilm), as indicated, and digestion was quenched by the addition of 1% formic acid.

The peptides were desalted using C18 tips (TopTip, GlyGen), dried and resuspended in 0.1% formic acid, and resolved by reversed-phase chromatography on 0.075 × 180-mm fused silica capillaries (J&W) packed with ReproSil reversed-phase material (Dr. Maisch, GmbH, Germany). The peptides were eluted with linear gradients of acetonitrile with 0.1% formic acid in water: 120 min of 5 to 28%, 15 min of 28 to 95%, and 25 min of 95% at flow rates of 0.15 μl/min. MS was performed using a Q Exactive HF-X mass spectrometer (Thermo Fisher Scientific) in a positive mode (mass/charge ratio, 300 to 1800; resolution, 120,000 for MS1 and 15,000 for MS2), and using repetitively full MS scan, followed by collision, induces dissociation (higher-energy collisional dissociation at 27 normalized collision energy) of the 18 most dominant ions (>1 charge) selected from the first MS scan. The automatic gain control settings were 3×10^6 for the full MS and 1×10^5 for the LC-MS/MS scans. The intensity threshold for triggering LC-MS/MS analysis was 1×10^4. A dynamic exclusion list was enabled with an exclusion duration of 20 s.

MS data were analyzed using the MaxQuant software 1.5.2.8 (*78*) for peak picking and identification using the Andromeda search engine, searching against the human proteome from the UniProt database with a mass tolerance of 6 parts per million (ppm) for the precursor masses and 20 ppm for the fragment ions. Oxidation on methionine and protein N terminus acetylation were accepted as variable modifications, and carbamidomethyl on cysteine was accepted as a static modification. Minimal peptide length was set to six amino acids, and a maximum of two miscleavages was allowed. The data were quantified by label-free analysis using the same software. Peptide- and protein-level false discovery rates (FDRs) were filtered to 1% using the target-decoy strategy. Protein tables were filtered to eliminate the identifications from the reverse database, common contaminants, and single-peptide identifications.

Statistical analysis of the identification and quantization results was done using Perseus 1.6.10.43 Software (*79*). Raw MS data are available via ProteomeXchange with the identifier PXD061770.

Calculation of cellular copy numbers

To calculate cellular copy numbers, Eq. 1 was used to determine relative iBAQ values (*36*, *37*) for each protein

$$\mathrm{riBAQ}(i) = \frac{\mathrm{iBAQ}(i)}{\text{Total iBAQ (sample)}} \quad (1)$$

where riBAQ(i) is the relative iBAQ value of protein i, iBAQ(i) is its iBAQ value as determined by MaxQuant, and Total iBAQ (sample) is the sum of all iBAQ values of the sample. Using Eq. 2, the mass (in grams) was calculated for each protein by multiplying riBAQ(i) by the total protein mass of the sample

$$m(i) = \text{riBAQ}(i) \times \text{Total mass}\left(\text{sample}\right) \quad (2)$$

The total number of moles present in the sample for a given protein was obtained using Eq. 3

$$n(i) = \frac{m(i)}{\text{MW}(i)} \quad (3)$$

where n is the total number of moles, m is the total mass of a given protein present in the sample, and MW is its molecular weight. The total number of molecules of a given protein present in the sample, $N(i)$, was then obtained using Avogadro's number (Eq. 4)

$$N(i) = n(i) \times 6.023 \times 10^{23} \quad (4)$$

Last, cellular copy numbers, $C(i)$, were determined using Eq. 5

$$C(i) = \frac{N(i)}{\text{Number of cells}} \quad (5)$$

where $N(i)$ is the total number of molecules obtained using Eq. 4 and the number of cells determined by colony counting.

Quantification using purified proteins standards

MetQ, FliY, BtuF, MetN, YecS, BtuD, MetI, and YecC were purified to >90% homogeneity, as previously described by our group (*41*, *43*). Five micrograms of each protein was digested by trypsin, following the method described above. To minimize technical variation, the proteins were combined in a mixture, containing 3.45×10^{-11} mol from each, and desalted. A mixture containing 3.45×10^{-12} mol from each protein was then analyzed by LC-MS/MS using a Thermo Fisher Scientific HF-X mass spectrometer. Data were processed using MaxQuant 2.4 with a 1% FDR, and all proteins were identified by at least six peptides. The ratio between the measured intensity of each purified protein and its known molar amount was used to convert the intensity measured in whole-cell samples into molar quantities. This molar amount was then compared to the value calculated using iBAQ quantification.

Membrane association assays

For the membrane association that studies only fresh cultures, ones that have not been frozen and/or stored were used. The experiments were conducted essentially as previously described (*41*, *80*), with the following modifications. Cells were transformed with an empty vector or with the same vector encoding the transporters YecSC, HisPQM, or BtuCD, as indicated. Cultures were grown in LB-ampicillin medium at 37°C with shaking to midexponential phase, and protein expression was induced by isopropyl β-D-1-thiogalactopyranoside (0.5 mM) for 1 hour. Cells were harvested and resuspended in 10 mM tris-HCl (pH 7.5) and 0.75 M sucrose. The cell suspension was then incubated on ice for 20 min in the presence of lysozyme (100 μg/ml; Amresco) and two volumes of 1.5 mM EDTA. The spheroplasts were then stabilized by the addition of 25 mM $MgCl_2$, and DNA originating form ruptured cells was digested with deoxyribonuclease I (100 μg/ml; Worthington). The spheroplasts were pelleted and resuspended in 100 mM tris-HCl (pH 7.5), 150 mM NaCl, and 5 mM $MgCl_2$ to an OD_{600} (optical density of 600 nm) of about 10 and kept on ice until use. Purified FLAG-tagged SBPs were added to the spheroplast suspension (160 nM BtuF, 5 μM FliY, and 15 μM HisJ), and following a 10-min incubation, unbound material was removed by 5-min centrifugation at 2500*g*. The amount of FLAG-tagged SBPs in the total, washed, and bound fractions was visualized using standard immunoblot procedures using an anti-FLAG M2 horseradish peroxidase–conjugate antibody (Sigma-Aldrich).

B_{12} utilization assays

This assay is based on the original protocol developed by the Kadner laboratory (*59*). In the *E. coli* Δ*metE* strain, methionine biosynthesis is solely catalyzed by MetH, a B_{12}-dependent methionine synthase. In this strain, growth is therefore dependent on the exogenous addition of either methionine or B_{12}. When the latter is supplied, growth fully depends on the uptake function of BtuCD-F (*59*). In the experiments shown in Fig. 8, $BtuF_{low}$ cells refer to Δ*metE* cells transformed with an empty vector, and $BtuF_{high}$ cells refer to the same cells transformed with a BtuF-encoding vector. Expression of the plasmid was not induced during the experiment, and, hence, excess BtuF in the $BtuF_{high}$ cells originates from promoter leakiness. As detailed in the text, this leaky expression amounts to 1000 to 2000 copies of BtuF per cell. Cultures were grown in LB media supplemented with kanamycin (50 μg/ml) and ampicillin (100 μg/ml) to mid-log phase and washed and resuspended in Davis minimal media to an OD_{600} of 0.05. Cultures (0.2 ml) were then grown in the absence or presence of methionine or B_{12}, as indicated. The OD of the cultures was measured every 5 min for 12 hours using an automated plate reader (Infinite M200 Pro, Tecan).

Supplementary Materials

The PDF file includes:

Figs. S1 to S8

Legends for tables S1 to S4

Other Supplementary Material for this manuscript includes the following:

Tables S1 to S4

REFERENCES AND NOTES

1. D. C. Rees, E. Johnson, O. Lewinson, ABC transporters: The power to change. *Nat. Rev. Mol. Cell Biol.* **10**, 218–227 (2009).
2. K. Kuchler, The ABC of ABCs: Multidrug resistance and genetic diseases. *FEBS J.* **278**, 3189 (2011).
3. A. Ersoy, B. Altintel, N. Livnat Levanon, N. Ben-Tal, T. Haliloglu, O. Lewinson, Computational analysis of long-range allosteric communications in CFTR. *eLife* **12**, RP88659 (2023).
4. C. A. McDevitt, A. D. Ogunniyi, E. Valkov, M. C. Lawrence, B. Kobe, A. G. McEwan, J. C. Paton, A molecular mechanism for bacterial susceptibility to zinc. *PLOS Pathog.* **7**, e1002357 (2011).
5. E. Vigonsky, I. Fish, N. Livnat-Levanon, E. Ovcharenko, N. Ben-Tal, O. Lewinson, Metal binding spectrum and model structure of the *Bacillus anthracis* virulence determinant MntA. *Metallomics* **7**, 1407–1419 (2015).
6. G. H. Scheepers, J. A. L. A. Nijeholt, B. Poolman, An updated structural classification of substrate-binding proteins. *FEBS Lett.* **590**, 4393–4401 (2016).
7. J. R. Wiśniewski, H. Koepsell, A. Gizak, D. Rakus, Absolute protein quantification allows differentiation of cell-specific metabolic routes and functions. *Proteomics* **15**, 1316–1325 (2015).
8. I. Cima, R. Schiess, P. Wild, M. Kaelin, P. Schüffler, V. Lange, P. Picotti, R. Ossola, A. Templeton, O. Schubert, T. Fuchs, T. Leippold, S. Wyler, J. Zehetner, W. Jochum, J. Buhmann, T. Cerny, H. Moch, S. Gillessen, R. Aebersold, W. Krek, Cancer genetics-guided discovery of serum biomarker signatures for diagnosis and prognosis of prostate cancer. *Proc. Natl. Acad. Sci. U.S.A.* **108**, 3342–3347 (2011).
9. J. A. Schäfer, S. Bozkurt, J. B. Michaelis, K. Klann, C. Münch, Global mitochondrial protein import proteomics reveal distinct regulation by translation and translocation machinery. *Mol. Cell* **82**, 435–446.e7 (2022).

10. K. L. Hickey, S. Swarup, I. R. Smith, J. C. Paoli, E. Miguel Whelan, J. A. Paulo, J. W. Harper, Proteome census upon nutrient stress reveals Golgiphagy membrane receptors. *Nature* **623**, 167–174 (2023).
11. A. Schmidt, K. Kochanowski, S. Vedelaar, E. Ahrné, B. Volkmer, L. Callipo, K. Knoops, M. Bauer, R. Aebersold, M. Heinemann, The quantitative and condition-dependent *Escherichia coli* proteome. *Nat. Biotechnol.* **34**, 104–110 (2016).
12. D. Nanavati, M. Gucek, J. L. S. Milne, S. Subramaniam, S. P. Markey, Stoichiometry and absolute quantification of proteins with mass spectrometry using fluorescent and isotope-labeled concatenated peptide standards. *Mol. Cell. Proteomics* **7**, 442–447 (2008).
13. C. Schmidt, C. Lenz, M. Grote, R. Lührmann, H. Urlaub, Determination of protein stoichiometry within protein complexes using absolute quantification and multiple reaction monitoring. *Anal. Chem.* **82**, 2784–2796 (2010).
14. A. Wepf, T. Glatter, A. Schmidt, R. Aebersold, M. Gstaiger, Quantitative interaction proteomics using mass spectrometry. *Nat. Methods* **6**, 203–205 (2009).
15. K. C. Tsolis, A. Economou, Chapter two - Quantitative proteomics of the *E. coli* membranome. *Methods Enzymol.* **586**, 15–36 (2017).
16. K. Krug, A. Carpy, G. Behrends, K. Matic, N. C. Soares, B. Macek, Deep coverage of the escherichia coli proteome enables the assessment of false discovery rates in simple proteogenomic experiments. *Mol. Cell. Proteomics* **12**, 3420–3430 (2013).
17. J. N. Adkins, H. M. Mottaz, A. D. Norbeck, J. K. Gustin, J. Rue, T. R. W. Clauss, S. O. Purvine, K. D. Rodland, F. Heffron, R. D. Smith, Analysis of the *Salmonella typhimurium* proteome through environmental response toward infectious conditions. *Mol. Cell. Proteomics* **5**, 1450–1461 (2006).
18. B. K. Chi, K. Gronau, U. Mäder, B. Hessling, D. Becher, H. Antelmann, *S*-bacillithiolation protects against hypochlorite stress in *Bacillus subtilis* as revealed by transcriptomics and redox proteomics. *Mol. Cell. Proteomics* **10**, M111.009506 (2011).
19. Z. M. Al-Majdoub, B. Achour, N. Couto, M. Howard, Y. Elmorsi, D. Scotcher, S. Alrubia, E. El-Khateeb, A.-M. Vasilogianni, N. Alohali, S. Neuhoff, L. Schmitt, A. Rostami-Hodjegan, J. Barber, Mass spectrometry-based abundance atlas of ABC transporters in human liver, gut, kidney, brain and skin. *FEBS Lett.* **594**, 4134–4150 (2020).
20. Z. M. Al-Majdoub, H. Al Feteisi, B. Achour, S. Warwood, S. Neuhoff, A. Rostami-Hodjegan, J. Barber, Proteomic quantification of human blood-brain barrier SLC and ABC transporters in healthy individuals and dementia patients. *Mol. Pharm.* **16**, 1220–1233 (2019).
21. J. Wissing, L. Jänsch, M. Nimtz, G. Dieterich, R. Hornberger, G. Kéri, J. Wehland, H. Daub, Proteomics analysis of protein kinases by target class-selective prefractionation and tandem mass spectrometry. *Mol. Cell. Proteomics* **6**, 537–547 (2007).
22. B. Fabre, T. Lambour, L. Garrigues, M. Ducoux-Petit, F. Amalric, B. Monsarrat, O. Burlet-Schiltz, M. P. Bousquet-Dubouch, Label-free quantitative proteomics reveals the dynamics of proteasome complexes composition and stoichiometry in a wide range of human cell lines. *J. Proteome Res.* **13**, 3027–3037 (2014).
23. M. A. Gillespie, C. G. Palii, D. Sanchez-Taltavull, P. Shannon, W. J. R. Longabaugh, D. J. Downes, K. Sivaraman, H. M. Espinoza, J. R. Hughes, N. D. Price, T. J. Perkins, J. A. Ranish, M. Brand, Absolute quantification of transcription factors reveals principles of gene regulation in erythropoiesis. *Mol. Cell* **78**, 960–974.e11 (2020).
24. N. M. Clarka, A. P. Fishera, B. Berckmansc, L. Van Den Broeck, E. C. Nelsona, T. T. Nguyena, E. Bustillo-Avendañod, S. G. Zebelle, M. A. Moreno-Risuenod, R. Simonc, K. L. Gallagherh, R. Sozzania, Protein complex stoichiometry and expression dynamics of transcription factors modulate stem cell division. *Proc. Natl. Acad. Sci. U.S.A.* **117**, 15332–15342 (2020).
25. P. Mehta, G. Jovanovic, T. Lenn, A. Bruckbauer, C. Engl, L. Ying, M. Buck, Dynamics and stoichiometry of a regulated enhancer-binding protein in live *Escherichia coli* cells. *Nat. Commun.* **4**, 1997 (2013).
26. P. D. Karp, S. Paley, R. Caspi, A. Kothari, M. Krummenacker, P. E. Midford, L. R. Moore, P. Subhraveti, S. Gama-Castro, V. H. Tierrafria, P. Lara, L. Muñiz-Rascado, C. Bonavides-Martinez, A. Santos-Zavaleta, A. Mackie, G. Sun, T. A. Ahn-Horst, H. Choi, M. W. Covert, J. Collado-Vides, I. Paulsen, The EcoCyc database (2023). *EcoSal Plus* **11**, eesp-0002-2023 (2023).
27. L. Arike, K. Valgepea, L. Peil, R. Nahku, K. Adamberg, R. Vilu, Comparison and applications of label-free absolute proteome quantification methods on *Escherichia coli*. *J. Proteomics* **75**, 5437–5448 (2012).
28. J. C. Wright, M. O. Collins, L. Yu, L. Käll, M. Brosch, J. S. Choudhary, Enhanced peptide identification by electron transfer dissociation using an improved mascot percolator. *Mol. Cell. Proteomics* **11**, 478–491 (2012).
29. T. Baba, T. Ara, M. Hasegawa, Y. Takai, Y. Okumura, M. Baba, K. A. Datsenko, M. Tomita, B. L. Wanner, H. Mori, Construction of *Escherichia coli* K-12 in-frame, single-gene knockout mutants: The Keio collection. *Mol. Syst. Biol.* **2**, 2006.0008 (2006).
30. M.-J. Han, S. Y. Lee, The *Escherichia coli* proteome: Past, present, and future prospects. *Microbiol. Mol. Biol. Rev.* **70**, 362–439 (2006).
31. H. Song, N. Lou, J. Liu, H. Xiang, D. Shang, Label-free quantitative proteomic analysis of the inhibition effect of *Lactobacillus rhamnosus* GG on *Escherichia coli* biofilm formation in co-culture. *Proteome Sci.* **19**, 4 (2021).
32. J. H. Weiner, L. Li, Proteome of the *Escherichia coli* envelope and technological challenges in membrane proteome analysis. *Biochim. Biophys. Acta* **1778**, 1698–1713 (2008).
33. X. Zhang, Less is more: Membrane protein digestion beyond urea-trypsin solution for next-level proteomics. *Mol. Cell. Proteomics* **14**, 2441–2453 (2015).
34. D. Samodova, C. M. Hosfield, C. N. Cramer, M. V. Giuli, E. Cappellini, G. Franciosa, M. M. Rosenblatt, C. D. Kelstrup, J. V. Olsen, ProAlanase is an effective alternative to trypsin for proteomics applications and disulfide bond mapping. *Mol. Cell. Proteomics* **19**, 2139–2157 (2020).
35. J. G. Meyer, S. Kim, D. A. Maltby, M. Ghassemian, N. Bandeira, E. A. Komives, Expanding proteome coverage with orthogonal-specificity α-lytic proteases. *Mol. Cell. Proteomics* **13**, 823–835 (2014).
36. J.-B. Shin, J. F. Krey, A. Hassan, Z. Metlagel, A. N. Tauscher, J. M. Pagana, N. E. Sherman, E. D. Jeffery, K. J. Spinelli, H. Zhao, P. A. Wilmarth, D. Choi, L. L. David, M. Auer, P. G. Barr-Gillespie, Molecular architecture of the chick vestibular hair bundle. *Nat. Neurosci.* **16**, 365–374 (2013).
37. J. F. Krey, P. A. Wilmarth, J.-B. Shin, J. Klimek, N. E. Sherman, E. D. Jeffery, D. Choi, L. L. David, P. G. Barr-Gillespie, Accurate label-free protein quantitation with high- and low-resolution mass spectrometers. *J. Proteome Res.* **13**, 1034–1044 (2014).
38. J. L. Radzikowski, S. Vedelaar, D. Siegel, Á. D. Ortega, A. Schmidt, M. Heinemann, Bacterial persistence is an active σ^S stress response to metabolic flux limitation. *Mol. Syst. Biol.* **12**, 882 (2016).
39. K. Valgepea, K. Adamberg, A. Seiman, R. Vilu, *Escherichia coli* achieves faster growth by increasing catalytic and translation rates of proteins. *Mol. BioSyst.* **9**, 2344–2358 (2013).
40. B. Soufi, K. Krug, A. Harst, B. Macek, Characterization of the *E. coli* proteome and its modifications during growth and ethanol stress. *Front. Microbiol.* **6**, 103 (2015).
41. O. Lewinson, A. T. Lee, K. P. Locher, D. C. Rees, A distinct mechanism for the ABC transporter BtuCD–BtuF revealed by the dynamics of complex formation. *Nat. Struct. Mol. Biol.* **17**, 332–338 (2010).
42. N. Tal, E. Ovcharenko, O. Lewinson, A single intact ATPase site of the ABC transporter BtuCD drives 5% transport activity yet supports full in vivo vitamin B_{12} utilization. *Proc. Natl. Acad. Sci. U.S.A.* **110**, 5434–5439 (2013).
43. S. Sabrialabe, J. G. Yang, O. Lewinson, E. Yariv, N. Ben-Tal, Substrate recognition and ATPase activity of the *E. coli* cysteine/cystine ABC transporter YecSC-FliY. *J. Biol. Chem.* **295**, 5245–5256 (2020).
44. P. T. Nguyen, J. Y. Lai, A. T. Lee, J. T. Kaiser, D. C. Rees, Noncanonical role for the binding protein in substrate uptake by the MetNI methionine ATP binding cassette (ABC) transporter. *Proc. Natl. Acad. Sci. U.S.A.* **115**, E10596–E10604 (2018).
45. G. F. Ames, C. E. Liu, A. K. Joshi, K. Nikaido, Liganded and unliganded receptors interact with equal affinity with the membrane complex of periplasmic permeases, a subfamily of traffic ATPases. *J. Biol. Chem.* **271**, 14264–14270 (1996).
46. M. K. Doeven, G. van den Bogaart, V. Krasnikov, B. Poolman, Probing receptor-translocator interactions in the oligopeptide ABC transporter by fluorescence correlation spectroscopy. *Biophys. J.* **94**, 3956–3965 (2008).
47. E. Vigonsky, E. Ovcharenko, O. Lewinson, Two molybdate/tungstate ABC transporters that interact very differently with their substrate binding proteins. *Proc. Natl. Acad. Sci. U.S.A.* **110**, 5440–5445 (2013).
48. M. R. Rohrbach, V. Braun, W. Köster, Ferrichrome transport in Escherichia coli K-12: Altered substrate specificity of mutated periplasmic FhuD and interaction of FhuD with the integral membrane protein FhuB. *J. Bacteriol.* **177**, 7186–7193 (1995).
49. J.-S. Woo, A. Zeltina, B. A. Goetz, K. P. Locher, X-ray structure of the *Yersinia pestis* heme transporter HmuUV. *Nat. Struct. Mol. Biol.* **19**, 1310–1315 (2012).
50. B. D. Bennett, E. H. Kimball, M. Gao, R. Osterhout, S. J. Van Dien, J. D. Rabinowitz, Absolute metabolite concentrations and implied enzyme active site occupancy in *Escherichia coli*. *Nat. Chem. Biol.* **5**, 593–599 (2009).
51. X.-P. Hu, H. Dourado, P. Schubert, M. J. Lercher, The protein translation machinery is expressed for maximal efficiency in *Escherichia coli*. *Nat. Commun.* **11**, 5260 (2020).
52. B. Görke, J. Stülke, Carbon catabolite repression in bacteria: Many ways to make the most out of nutrients. *Nat. Rev. Microbiol.* **6**, 613–624 (2008).
53. R. Milo, P. Jorgensen, U. Moran, G. Weber, M. Springer, BioNumbers—The database of key numbers in molecular and cell biology. *Nucleic Acids Res.* **38**, D750–D753 (2009).
54. C. C. Wu, J. R. Yates III, The application of mass spectrometry to membrane proteomics. *Nat. Biotechnol.* **21**, 262–267 (2003).
55. N. Solis, S. J. Cordwell, Current methodologies for proteomics of bacterial surface-exposed and cell envelope proteins. *Proteomics* **11**, 3169–3189 (2011).
56. O. Lewinson, N. Livnat-Levanon, Mechanism of action of ABC importers: Conservation, divergence, and physiological adaptations. *J. Mol. Biol.* **429**, 606–619 (2017).
57. G. W. Li, D. Burkhardt, C. Gross, J. S. Weissman, Quantifying absolute protein synthesis rates reveals principles underlying allocation of cellular resources. *Cell* **157**, 624–635 (2014).
58. R. J. Kadner, Transport systems for L-methionine in *Escherichia coli*. *J. Bacteriol.* **117**, 232–241 (1974).

59. N. Cadieux, C. Bradbeer, E. Reeger-Schneider, W. Köster, A. K. Mohanty, M. C. Wiener, R. J. Kadner, Identification of the periplasmic cobalamin-binding protein BtuF of *Escherichia coli*. *J. Bacteriol.* **184**, 706–717 (2002).
60. F. A. Quiocho, J. C. Spurlino, L. E. Rodseth, Extensive features of tight oligosaccharide binding revealed in high-resolution structures of the maltodextrin transport/chemosensory receptor. *Structure* **5**, 997–1015 (1997).
61. I. Ohtsu, N. Wiriyathanawudhiwong, S. Morigasaki, T. Nakatani, H. Kadokura, H. Takagi, The L-cysteine/L-cystine shuttle system provides reducing equivalents to the periplasm in *Escherichia coli*. *J. Biol. Chem.* **285**, 17479–17487 (2010).
62. N. S. Kadaba, J. T. Kaiser, E. Johnson, A. Lee, D. C. Rees, The high-affinity *E. coli* methionine ABC transporter: Structure and allosteric regulation. *Science* **321**, 250–253 (2008).
63. A. Sirko, M. Zatyka, E. Sadowy, D. Hulanicka, Sulfate and thiosulfate transport in *Escherichia coli* K-12: Evidence for a functional overlapping of sulfate- and thiosulfate-binding proteins. *J. Bacteriol.* **177**, 4134–4136 (1995).
64. E. L. Borths, B. Poolman, R. N. Hvorup, K. P. Locher, D. C. Rees, In vitro functional characterization of BtuCD-F, the *Escherichia coli* ABC transporter for vitamin B_{12} uptake. *Biochemistry* **44**, 16301–16309 (2005).
65. M. Yang, N. Livnat Levanon, B. Acar, B. Aykac Fas, G. Masrati, J. Rose, N. Ben-Tal, T. Haliloglu, Y. Zhao, O. Lewinson, Single-molecule probing of the conformational homogeneity of the ABC transporter BtuCD. *Nat. Chem. Biol.* **14**, 715–722 (2018).
66. N. Livnat-Levanon, A. I. Gilson, N. Ben-Tal, O. Lewinson, The uncoupled ATPase activity of the ABC transporter $BtuC_2D_2$ leads to a hysteretic conformational change, conformational memory, and improved activity. *Sci. Rep.* **6**, 21696 (2016).
67. T. Kalwarczyk, M. Tabaka, R. Holyst, Biologistics—Diffusion coefficients for complete proteome of *Escherichia coli*. *Bioinformatics* **28**, 2971–2978 (2012).
68. J. Alfonso-Garrido, E. Garcia-Calvo, J. L. Luque-Garcia, Sample preparation strategies for improving the identification of membrane proteins by mass spectrometry. *Anal. Bioanal. Chem.* **407**, 4893–4905 (2015).
69. C. Merlin, G. Gardiner, S. Durand, M. Masters, The *Escherichia coli metD* locus encodes an ABC transporter which includes Abc (MetN), YaeE (MetI), and YaeC (MetQ). *J. Bacteriol.* **184**, 5513–5517 (2002).
70. M. L. Carlson, R. G. Stacey, J. W. Young, I. S. Wason, Z. Zhao, D. G. Rattray, N. Scott, C. H. Kerr, M. Babu, L. J. Foster, F. D. Van Hoa, Profiling the *Escherichia coli* membrane protein interactome captured in peptidisc libraries. *eLife* **8**, e46615 (2019).
71. M. L. Oldham, J. Chen, Snapshots of the maltose transporter during ATP hydrolysis. *Proc. Natl. Acad. Sci. U.S.A.* **108**, 15152–15156 (2011).
72. M. D. Manson, W. Boos, P. J. Bassford Jr., B. A. Rasmussen, Dependence of maltose transport and chemotaxis on the amount of maltose-binding protein. *J. Biol. Chem.* **260**, 9727–9733 (1985).
73. H. Bedouelle, P. J. Bassford Jr., A. V. Fowler, I. Zabin, J. Beckwith, M. Hofnung, Mutations which alter the function of the signal sequence of the maltose binding protein of *Escherichia coli*. *Nature* **285**, 78–81 (1980).
74. E. L. Borths, K. P. Locher, A. T. Lee, D. C. Rees, The structure of *Escherichia coli* BtuF and binding to its cognate ATP binding cassette transporter. *Proc. Natl. Acad. Sci. U.S.A.* **99**, 16642–16647 (2002).
75. N. K. Karpowich, H. H. Huang, P. C. Smith, J. F. Hunt, Crystal structures of the BtuF periplasmic-binding protein for vitamin B12 suggest a functionally important reduction in protein mobility upon ligand binding. *J. Biol. Chem.* **278**, 8429–8434 (2003).
76. S. I. Patzer, K. Hantke, The zinc-responsive regulator Zur and its control of the*znu* gene cluster encoding the ZnuABC zinc uptake system in *Escherichia coli*. *J. Biol. Chem.* **275**, 24321–24332 (2000).
77. K. De Pina, V. Desjardin, M. A. Mandrand-Berthelot, G. Giordano, L. F. Wu, Isolation and characterization of the *nikR* gene encoding a nickel-responsive regulator in *Escherichia coli*. *J. Bacteriol.* **181**, 670–674 (1999).
78. J. Cox, M. Mann, MaxQuant enables high peptide identification rates, individualized p.p.b.-range mass accuracies and proteome-wide protein quantification. *Nat. Biotechnol.* **26**, 1367–1372 (2008).
79. S. Tyanova, T. Temu, P. Sinitcyn, A. Carlson, M. Y. Hein, T. Geiger, M. Mann, J. Cox, The Perseus computational platform for comprehensive analysis of (prote)omics data. *Nat. Methods* **13**, 731–740 (2016).
80. H. Qasem-Abdullah, M. Perach, N. Livnat-Levanon, O. Lewinson, ATP binding and hydrolysis disrupt the high-affinity interaction between the heme ABC transporter HmuUV and its cognate substrate-binding protein. *J. Biol. Chem.* **292**, 14617–14624 (2017).

Acknowledgments: Figures 9 and 10 were created using BioRender.com. **Funding:** O.L. was supported by grants from NATO Science for Peace and Security Program (SPS project G5685), the Rappaport institute for biomedical research, and the Israeli Academy of Sciences project 1006/18. **Author contributions:** Conceptualization: O.L. Methodology: H.Q.A., M.P., M.G., N.L.L., T.Z., and O.L. Investigation: H.Q.A., M.P., M.G., N.L.L., T.Z., and O.L. Analysis: H.Q.A, M.P., T.Z., and O.L. Writing, review, and editing: H.Q.A., M.P., M.G., N.L.L., T.Z., and O.L. **Competing interests:** The authors declare that they have no competing interests. **Data and materials availability:** All data needed to evaluate the conclusions in the paper are present in the paper and/or the Supplementary Materials.

Submitted 10 July 2024
Accepted 16 April 2025
Published 21 May 2025
10.1126/sciadv.adq7470